IEEE Access
Multidisciplinary | Rapid Review | Open Access Journal

Received December 10, 2020, accepted December 22, 2020, date of publication January 14, 2021, date of current version January 27, 2021.

Digital Object Identifier 10.1109/ACCESS.2021.3051664

Mitigation of PA Nonlinearity for IEEE 802.11ah Power-Efficient Uplink via Iterative Subcarrier Regularization

LI CHO[1], (Member, IEEE), XIANHUA YU[1], (Student Member, IEEE), CHAU-YUN HSU[1,2], (Member, IEEE), AND PIN-HAN HO[3], (Fellow, IEEE)

[1]Center of Broadband Technology, Tatung University, Taipei 10452, Taiwan
[2]Department of Electrical Engineering, Tatung University, Taipei 10452, Taiwan
[3]Department of Electrical and Computer Engineering, University of Waterloo, Waterloo, ON N2L 3G1, Canada

Corresponding author: Li Cho (lcho@gm.ttu.edu.tw)

ABSTRACT An orthogonal frequency division multiplexing (OFDM) transmitter for 802.11ah uplink may consume unnecessarily high power due to the malicious effect of a large peak-to-average power ratio (PAPR). This is particularly a problem for client devices (CDs) under the low-power wide-area (LPWA) technology in an Internet of thing (IoT) system, where high PAPR signals may drive the power amplifier (PA) to operate with large input back-off (IBO). This article focuses on receiver-side signal compensation (SC) techniques and introduces a novel scheme called iterative subcarrier regularization (ISR), which is based on the generalization of Papoulis-Gerchberg algorithm (GPGA). We claim that the proposed scheme is completely compatible with 802.11ah as it only exploits the prior information available in the standard operations and popular system-build-in functions in the iterative signal reconstruction process. Extensive numerical evaluations demonstrate that the proposed scheme can improve PA efficiency by 4–9 dB for uplink signaling.

INDEX TERMS Orthogonal frequency division multiplexing (OFDM), nonlinear noise, Papoulis-Gerchberg algorithm, peak-to-average power ratio (PAPR), 802.11ah.

I. INTRODUCTION

Low-power wide-area (LPWA) technologies have captured great attentions from both industry and academia in the last decade due to the fast-pace deployment of internet of things (IoT) [1]. As a major service provisioned under the category of machine-type communication (MTC) in both licensed and unlicensed band, the IoT systems under LPWA have to support the interconnection of miniature and low-cost devices with long-range transmission and low power consumption [2], [3].

SigFox and long range (LoRa) were firstly announced as commercial LPWA technologies and have been significantly deployed in many countries within the last decade [1]. This has triggered the Third Generation Partnership Project (3GPP) and IEEE to rapidly complete the standardization of narrowband (NB)-IoT [4] and 802.11ah (Wi-Fi HaLow) [5], respectively, in order to be involved with great IoT market. NB-IoT can be directly applied to GSM or LTE system for reducing deployment costs and thus, many industries (e.g., Nokia, Ericsson, and Huawei) have spent tremendous effort on its standardization [6]. On the other hand, 802.11ah is highly compatible to the existing Wi-Fi systems due to the analogous numerology to IEEE 802.11ac, which utilizes unlicensed industrial, scientific and medical (ISM) radio bands for transmission. It has been well reported that both emerging LPWA technologies on licensed and unlicensed bands are quite competitive and demonstrate remarkable deployment superiority [5].

Although OFDM yields high spectral efficiency, it is subject to unnecessarily high power consumption due to possibly high peak-to-average power ratio (PAPR) that may significantly damage the efficiency of the power amplifier (PA) [7]. Note that power efficiency is one of the most critical requirements for those energy-hungry IoT client devices (CDs).

The associate editor coordinating the review of this manuscript and approving it for publication was Donatella Darsena.

To avoid high PAPR, various design aspects and novel schemes are reported for both NB-IoT and 802.11ah, respectively. NB-IoT allows single-carrier transmissions via discrete Fourier transform (DFT) spread OFDM (DFT-s-OFDM) for uplink to make the CD simple and free from high PAPR, and for any multi-carrier transmission, the number of subcarriers is limited to 12 (1 Physical Resource Block, PRB) [8]. For 802.11ah, most of the power saving methods in literature were proposed in the circuit [9]–[11] or medium access control (MAC) level [12]–[15], while a system-level method, to the best of our knowledge, can only be found in [16] that considers the scenario of a low-cost low-power transmitter communicating with a high-quality access point (AP). By compensating for the nonlinearity of received signals at the AP, the input back-off (IBO) of CD's PA can be minimized according to the spectral mask and channel quality [17].

There are numerous advantages by employing such a receiver-side compensation based solution, which are summarized in the following three aspects.

- *Support of MTC type Applications.* Since MTC acts as a delay-tolerance service, almost all LPWA technologies allow a long duration of idle/sleep mode for power saving. The burst traffic nature caused by the event-driven wireless sensor networks (WSN) [18] brings a manageable time margin for performing the iterative computations at the AP.
- *Low-cost and simple design for IoT-CDs.* A common design principle for an IoT system is to leave all possible complicated operations performed at the AP while making the IoT CDs as simple as possible. For example, several efficient distortionless-based PAPR reduction schemes still require multiple times of fast Fourier transform (FFT) size of computation to generate low-PAPR signal candidates for UL transmission [19], [20]. Even the simplest clipping and filtering PAPR reduction [21] may consume larger than two times power consumption due to the repeated and oversampled FFT/inverse FFT (IFFT) operations. Although the signal recovery could be seriously degraded due to imprecision of channel estimation [22], the receiver-side linearization methods follow the simple CD principle and thus are very suitable to the MTC transmissions, where the CDs are with zero or limited user mobility [23], leading to minimum estimation error of channel state information (CSI).
- *Uplink (UL)-dominated IoT-CD traffics.* The receiver-side signal linearization approaches are particularly suitable for MTC type systems where the IoT-CD traffics are UL-dominated [18].

With the abovementioned advantages, the studies on receiver-side compensation have been extensively reported in literature in the following two categories: (1) maximum-likelihood (ML) detection-based (e.g., [24]–[26]), and (2) signal compensation (SC)-based (e.g.,[27]–[30]). The former can achieve a better bit error rate (BER) performance than the latter at the expense of exponentially growing computational complexity with the FFT size that leads to infeasibility. On the other hand, although those reported SC schemes require significantly less computation effort, to the best of our knowledge, all of them take the data-subcarrier-only signal model which is far from any real-world specification/standard. Note that the actual OFDM system contains non-data-bearing subcarriers such as pilot and null subcarriers. The use of data-subcarrier-only signal model would lose the benefits brought by prior information in specification/standard. In addition, as most reported SC schemes are based on *iterative clipping noise cancellation* (ICNC) [27], their transmit signals require multiple clipping and filtering (CF) operations to achieve a targeted PAPR, and the peak regrowth still suffers from the PA nonlinearity otherwise [21]. Such repeated CF certainly brings up additional computational complexity to the transmitter in IoT-CDs.

In this article, we propose a novel SC scheme termed *iterative subcarrier regularization* (ISR) to helps the IoT-CDs to transmit signals with lower IBO for power saving. The proposed ISR is featured by a direct compensation of the PA nonlinearity at the OFDM receiver, instead of taking the CF-based approach that needs to be initiated at the transmitter. To this end, the proposed ISR scheme takes Papoulis-Gerchberg Algorithm (PGA) [31], [32] as basis while further considering specified subcarrier information, so as to enable an effective reconstruction of signal vector at the receiver. Based on the generalization of PGA (GPGA) [33], [34] and decision-aided reconstruction (DAR) [35], the proposed ISR scheme can simply regularize the subcarrier data in the frequency domain, which leads to a very light-weight signal linearization process that can be implemented via system-built-in functions of a typical OFDM receiver, thus yielding high compatibility with the current industry specification/standard. The simulation results demonstrate that the proposed ISR scheme can solidly improve the BER performance of the distorted signal caused by the presence of PA nonlinearity.

The rest of the article is organized as follows. In Section II, the system and signal model of the OFDM-based IoT transceiver is presented. Section III presents the proposed ISR scheme along with its evaluation of computational complexity and restoration performance. Section IV provides the simulation results. Section V concludes the article.

Notation: Boldface letters denote matrices or column vectors. Superscripts, $[\cdot]^{-1}$, $[\cdot]^{T}$, and $[\cdot]^{H}$ stand for matrix inversion operation, transpose, and Hermitian transpose, respectively. $\mathbb{E}\{\cdot\}$ is the expectation operator. $\boldsymbol{I_k}$ denotes the $k \times k$ identity matrix. $diag\{\boldsymbol{x}\}$ returns a diagonal matrix with $\boldsymbol{x}$ on its diagonal. $\mathcal{CN}\left(0,\sigma^2\right)$ represents the distribution of circularly symmetric complex Gaussian random variable with zero mean and variance σ^2. $\|\boldsymbol{x}\|_2$ denotes the Euclidean norm of a vector $\boldsymbol{x}$.

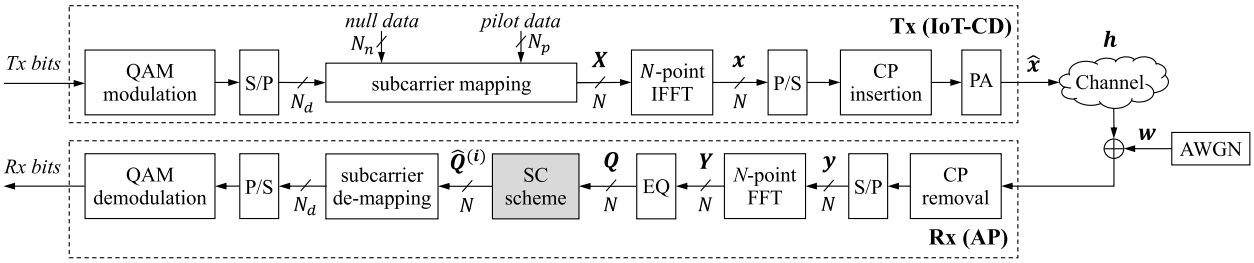

FIGURE 1. Baseband block diagram of specification-based OFDM transceiver with SC schemes.

II. SYSTEM AND SIGNAL MODEL

Fig. 1 presents the baseband block diagram of a generic SC-based OFDM transceiver. Let $\boldsymbol{X} = [X_0, \ldots, X_{N-1}]^T$ denote the subcarrier vector that carries N_d quadrature amplitude modulation (QAM) data, N_p pilot data and N_n null data (including guard band and DC). The time-domain OFDM symbol vector can be generated by $\boldsymbol{x} \triangleq [x_0, \ldots, x_{N-1}]^T = \boldsymbol{\mathcal{F}_N^H X}$, where $\boldsymbol{\mathcal{F}_N}$ is the N-by-N DFT matrix whose entry is given by

$$[\boldsymbol{\mathcal{F}_N}]_{(n,k)} = \frac{1}{\sqrt{N}} e^{-j\left(\frac{2\pi}{N}\right)nk} \quad , 0 \le n, k \le N-1. \tag{1}$$

A cyclic prefix (CP) with length P is inserted into $\boldsymbol{x}$ to mitigate the inter-symbol interference, yielding $[x_{N-P}, \ldots, x_{N-1}, x_0, \ldots, x_{N-1}]^T$. Considering the Rapp model [36], the transmitted sequence can be expressed as

$$\hat{\boldsymbol{x}} = G(\boldsymbol{x}) = g \cdot \boldsymbol{x} \left[1 + \left(\frac{g \cdot |\boldsymbol{x}|}{A_{sat}} \right)^{2p} \right]^{-\frac{1}{2p}}, \tag{2}$$

where A_{sat} is the PA saturation level specified by the value of IBO (in dB) from $A_{sat} = x_{RMS} \cdot 10^{IBO/20}$, $x_{RMS} = \sqrt{\sum_{n=0}^{N-1} |x_n|^2 / N}$, p is the smoothness factor, and g is the amplifier voltage gain. Here, we consider a unitary gain ($g = 1$) for simplicity and generality and a severe nonlinearity ($p = 2$) for simulating the low-complexity PA of IoT-CD.

Assuming a perfect synchronization and channel estimation, the received samples over the Rayleigh fading channel and after CP removal is given by

$$\boldsymbol{y} = \boldsymbol{h} \circledast_N \hat{\boldsymbol{x}} + \boldsymbol{w}, \tag{3}$$

where $\boldsymbol{h} = [h_0, \ldots, h_{L-1}]^T$ is the L-tap channel impulse response ($L \le P$), $\circledast_N$ is the circular convolution operator with length N, and $\boldsymbol{w} = [w_0, \ldots, w_{N-1}]^T$ is an additive white Gaussian noise (AWGN) vector whose elements follow $w_n \sim \mathcal{CN}(0, \sigma^2)$. Thus, we have the received subcarrier data vector:

$$\boldsymbol{Y} = \boldsymbol{H}\hat{\boldsymbol{X}} + \boldsymbol{W}, \tag{4}$$

where $H = diag\left\{\boldsymbol{\mathcal{F}_N h^0}\right\}$ is the channel frequency response, $\boldsymbol{h^0} = [\boldsymbol{h}, 0, \ldots, 0]^T$ is the zero-padded $\boldsymbol{h}$ with length N, and $\boldsymbol{Y}, \hat{\boldsymbol{X}}$ and $\boldsymbol{W}$ are the DFT of $\boldsymbol{y}, \hat{\boldsymbol{x}}$ and $\boldsymbol{w}$, respectively. From (4), the equalized subcarrier data vector can be written as

$$\boldsymbol{Q} = \boldsymbol{YH^{-1}} = \boldsymbol{H}\hat{\boldsymbol{X}}\boldsymbol{H^{-1}} + \boldsymbol{WH^{-1}}. \tag{5}$$

After employing an SC scheme on $\boldsymbol{Q}$, the i iteration- reconstructed subcarrier data vector $\hat{\boldsymbol{Q}}^{(\boldsymbol{i})} = \left[\hat{Q}_0^{(i)}, \ldots, \hat{Q}_{N-1}^{(i)}\right]^T$ is obtained for a better result of QAM demodulation.

III. PROPOSED SC SCHEME

In this section, the process for PGA generalization is firstly presented, followed by the two crucial parts of the proposed ISR scheme, including the prior knowledge on time (data) and frequency (transformed) domain, are described. Then we present the analysis of the proposed ISR scheme.

A. PROPOSED EXTENDED PAPOULIS-GERCHBERG ALGORITHM

PGA has been taken as a well-known tool for restoration of bandlimited signals [37]; however, we introduce GPGA to handle a general signal [33], [34].

A discrete signal with M samples can be described by an M-dimensional complex vector $\boldsymbol{v} = [v_0, \ldots, v_{M-1}]^T$, $v_n \in \mathbb{C}^M$, and its known sample vector is defined as

$$\boldsymbol{K_D} = \boldsymbol{\mathfrak{I}_D v}, \tag{6}$$

where $\boldsymbol{\mathfrak{I}_D}$ is an M-by-M diagonal matrix with binary coefficients on its diagonal: $[\boldsymbol{\mathfrak{I}_D}]_{(j,j)} = 1$ if the j-th sample in data domain is known and $[\boldsymbol{\mathfrak{I}_D}]_{(j,j)} = 0$ otherwise. We denote the number of the known samples as $M_D \in \{0, \ldots, M\}$, thus the lost-knowledge ratio of data domain is $\mathcal{L}_D = 1 - M_D/M$.

In the transformed domain, the DFT of the signal $\boldsymbol{v}$ is the vector $\boldsymbol{V} \in \mathbb{C}^M$ given by $\boldsymbol{V} = \boldsymbol{\mathcal{F}_M v}$. Its prior knowledge vector can be written as

$$\boldsymbol{K_T} = \boldsymbol{\mathfrak{I}_T V}, \tag{7}$$

where $\boldsymbol{\mathfrak{I}_T}$ is an M-by-M diagonal matrix with binary coefficients on its diagonal: $[\boldsymbol{\mathfrak{I}_T}]_{(j,j)} = 1$ if the j-th sample in transformed domain is known and $[\boldsymbol{\mathfrak{I}_T}]_{(j,j)} = 0$ otherwise. Also, we denote the number of the known samples as $M_T \in \{0, \ldots, M\}$, and the knowledge ratio of transformed domain is $\mathcal{K}_T = M_T/M$. According to [33], the lost sample reconstruction with perfect known samples can be achieved if $\mathcal{L}_D \le \mathcal{K}_T$ is satisfied. The algorithm starts with $\hat{\boldsymbol{v}}^{(\boldsymbol{i}=\boldsymbol{0})} = \boldsymbol{K_D}$, where iteration number i is set to zero as an initial guess. Then, the iterative process consists of following three steps:

1. Apply the transformed-domain partial knowledge $\boldsymbol{K_T}$ to $\hat{\boldsymbol{v}}^{(i)}$:

$$\hat{\boldsymbol{v}}^{(i+1)} = \mathcal{F}_M^H \left[(\boldsymbol{I} - \mathcal{I}_T)\, \mathcal{F}_M \hat{\boldsymbol{v}}^{(i)} + \boldsymbol{K_T} \right]. \tag{8}$$

2. Replace known samples in the estimated $\hat{v}^{(i+1)}$:

$$\hat{\boldsymbol{v}}^{(i+1)} = (\boldsymbol{I} - \mathcal{I}_D)\, \hat{\boldsymbol{v}}^{(i+1)} + \boldsymbol{K_D}. \tag{9}$$

3. Verify if the process converged to the specified threshold δ based on the normalized mean square error (NMSE), i.e.,

$$NMSE\left(\hat{\boldsymbol{v}}^{(i)}\right) = \frac{\left\| \hat{\boldsymbol{v}}^{(i)} - \hat{\boldsymbol{v}}^{(i+1)} \right\|_2^2}{\left\| \hat{\boldsymbol{v}}^{(i)} \right\|_2^2} < \delta. \tag{10}$$

If not, return to the first step with $i = i + 1$.

B. FREQUENCY-DOMAIN PRIOR KNOWLEDGE

The knowledge of the transformed domain, viz., frequency domain, is referred to as the subcarrier mapping described in 802.11ah standard [5], which consists of data, pilot, and null subcarriers (i.e., guard and DC subcarriers), with options of carrier bandwidth (CBW) including 1, 2, 4, 8, and 16 MHz. Throughout this article, we use CBW1 (1 MHz) parameterization to demonstrate the proposed algorithm, where its subcarrier mapping is illustrated in Fig. 2.

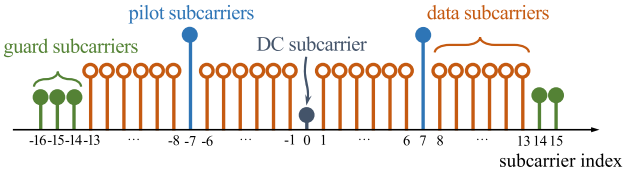

FIGURE 2. Frequency-domain prior knowledge from the subcarrier mapping based on the 802.11ah standard (CBW1 parameterization).

A very unique design of the proposed ISR is that it only takes the protocol operation parameters of 802.11ah, including the values of pilot and null subcarriers, as the frequency-domain prior knowledge (denote as solid dots in Fig. 2) and inputs of the rule-based GPGA. Accordingly, the first step of ISR can be described by rewriting (8) as

$$\hat{\boldsymbol{q}}^{(i+1)} = \mathcal{F}_N^H \left[\left(\boldsymbol{I} - \mathcal{I}_T^{ISR} \right) \hat{\boldsymbol{Q}}^{(i)} + \boldsymbol{K}_T^{ISR} \right], \tag{11a}$$

where N is the FFT size, $\hat{\boldsymbol{q}}^{(i)} = \mathcal{F}_N^H \hat{\boldsymbol{Q}}^{(i)}$, $\boldsymbol{K}_T^{ISR}$ is the prior knowledge vector according to the standard (the example vector for CBW1 parameterization is given in Table 1), and $\mathcal{I}_T^{ISR}$ is an N-by-N matrix with binary coefficients on its diagonal: $\left[\mathcal{I}_T^{ISR}\right]_{(j,j)} = 1$ if the j-th frequency component is a pilot or null subcarrier and $\left[\mathcal{I}_T^{ISR}\right]_{(j,j)} = 0$ otherwise. In this case, the ratio of the prior knowledge is $\mathcal{K}_T^{ISR} = (N_p + N_n)/N = (6+2)/32 = 25\%$, which implies a successful reconstruction of an incomplete signal vector cannot exceed 25% lost samples according to [33].

TABLE 1. 802.11ah (CBW1)-Based Frequency-Domain Prior Knowledge[1]

vector index	carrier index	value	carrier type	vector index	carrier index	value	carrier type
0	0	0	DC	16	-16	0	guard
1	1	$\mathcal{M}$kinds	data	17	-15	0	guard
⋮	⋮	⋮	⋮	18	-14	0	guard
6	6	$\mathcal{M}$kinds	data	19	-13	$\mathcal{M}$kinds	data
7	7	1	pilot[2]	⋮	⋮	⋮	⋮
8	8	$\mathcal{M}$kinds	data	24	-8	$\mathcal{M}$kinds	data
⋮	⋮	⋮	⋮	25	-7	-1	pilot[2]
13	13	$\mathcal{M}$kinds	data	26	-6	$\mathcal{M}$kinds	data
14	14	0	guard	⋮	⋮	⋮	⋮
15	15	0	guard	31	-1	$\mathcal{M}$kinds	data

[1]Deterministic and probabilistic prior information is denoted in red and blue, respectively.
[2]The position of pilot subcarriers may change in each OFDM slot for performing "traveling pilots".

On the other hand, though the received data subcarriers herein are taken as unknown part and do not contribute to the reconstruction process in each iteration (denote as hollow dots in Fig. 2), they actually carry the probabilistic prior knowledge of $\mathcal{M}$-ary constellation mapping that may help the subsequent SC. Such a concept was firstly report in DAR [35] where all PSK/QAM symbols were performed hard decision iteratively for SC. To combine the DAR process, the action of applying frequency-domain prior knowledge can be re-expressed as the so-called ISR:

$$\hat{\boldsymbol{q}}^{(i+1)} = \mathcal{F}_N^H \left[\left(\boldsymbol{I} - \mathcal{I}_T^{ISR} \right) \boldsymbol{Q}_{HD}^{(i)} + \boldsymbol{K}_T^{ISR} \right], \tag{11b}$$

where

$$\hat{\boldsymbol{Q}}_{HD}^{(i)} = \underset{X \in \mathcal{M}-\mathrm{QAM}}{\arg\min} \left(\left\| \hat{\boldsymbol{Q}}^{(i)} - \boldsymbol{X} \right\|_2 \right), \quad \hat{\boldsymbol{Q}}^{(i)} \in \text{ data subcarriers}. \tag{11c}$$

For the convenience, we call (11a) as ISR scheme I (ISR-I) and (11b) as ISR scheme II (ISR-II) in the rest of the article. Their performance comparison and discussion will be provided in Section III-E.

C. TIME-DOMAIN PRIOR KNOWLEDGE

Since nonlinear noise on a time-domain OFDM symbol is mainly caused by large-amplitude samples owing to the severe saturation, it is reasonable to retain the low-amplitude samples in each iteration as time-domain prior knowledge. As illustrated in Fig. 3, the severely-saturated samples are taken as the lost ones that needs reconstruction by calculating the estimated saturation level:

$$\hat{A}_{sat} = q_{RMS} \cdot 10^{IBO/20}, \tag{12}$$

where IBO is the value of IBO in dB used in the transmission known in advance by the receiver, and $q_{RMS} = \sqrt{\sum_{n=0}^{N-1} |q_n|^2 / N}$, $q_n \in \boldsymbol{q}$, $\boldsymbol{q} = \mathcal{F}_N^H \boldsymbol{Q}$. The known sample determination can be achieved by creating the

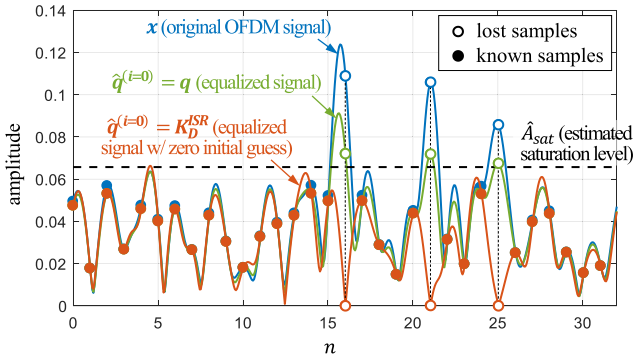

FIGURE 3. Lost samples determination and initial guess settings for the saturated signal in time domain.

denotation matrix:

$$\left[\mathfrak{I}_D^{ISR}\right]_{(j,j)} = \begin{cases} 1, & q_n < \hat{A}_{sat} \\ 0, & q_n \geq \hat{A}_{sat} \end{cases}, 0 \leq j, n \leq N-1. \quad (13)$$

As a result of (6) and (13), the time-domain prior knowledge of the proposed ISR scheme can be obtained by

$$\boldsymbol{K}_D^{ISR} = \mathfrak{I}_D^{ISR}\boldsymbol{q}. \quad (14)$$

Note that $\boldsymbol{K}_D^{ISR}$ herein still suffers from relatively-low nonlinearity, but can be improved by linearization techniques such as digital predistortion [38] if affordable by an IoT device.

Since the saturated signals are highly correlated with their original samples, they can be taken as the best initial guesses (instead of using zero samples as in the original GPGA) in the restoration process. Note that inserting zero samples is a highly nonlinear process that reduces the smoothness of a signal and introduces much in-band and out-of-band noises. Therefore, as shown in Fig. 3, the proposed algorithm starts with $\hat{\boldsymbol{q}}^{(i=0)} = \boldsymbol{q}$ (green hollow dots) instead of $\hat{\boldsymbol{q}}^{(i=0)} = \boldsymbol{K}_D^{ISR}$ (orange hollow dots). We will indicate in Section III-E that using the equalized samples as the initial guess can significantly accelerate the convergence compared with the case of using zeros.

By (13), the time-domain lost-knowledge ratio can be expressed by $\mathcal{L}_D^{ISR} = 1 - N_D/N$, where $N_D \in \{0, \ldots, N\}$ is the number of ones in $\mathfrak{I}_D^{ISR}$. Since the proposed ISR works under the criterion $\mathcal{L}_D^{ISR} \leq \mathcal{K}_T^{ISR}$ [33], the value of $\mathcal{L}_D^{ISR}$, which is dominated by the IBO of the transmit PA according to (12), can be used to estimate the recovery limitation. To this end, we perform Monte Carlo simulations with 5×10^5 random OFDM symbols to obtain the complementary cumulative distribution function (CCDF) of 802.11ah received samples suffered from a different extent of nonlinearity. Fig. 4(a) and 4(b) shows the CCDF of the amplitude for signal $\boldsymbol{q}$ over the poor ($E_b/N_0 = 0$ dB) and good ($E_b/N_0 = 20$ dB) wireless channel, respectively, where E_b/N_0 is the normalized signal-to-noise ratio (SNR). It can be clearly found that decreasing the IBO would increase $\mathcal{L}_D^{ISR}$ under any channel quality. Table 2 provides more results of $\mathcal{L}_D^{ISR}$ with/without the channel noise ($E_b/N_0 = 0, 5, 10, 15, 20$ dB) for $IBO = 08$ dB.

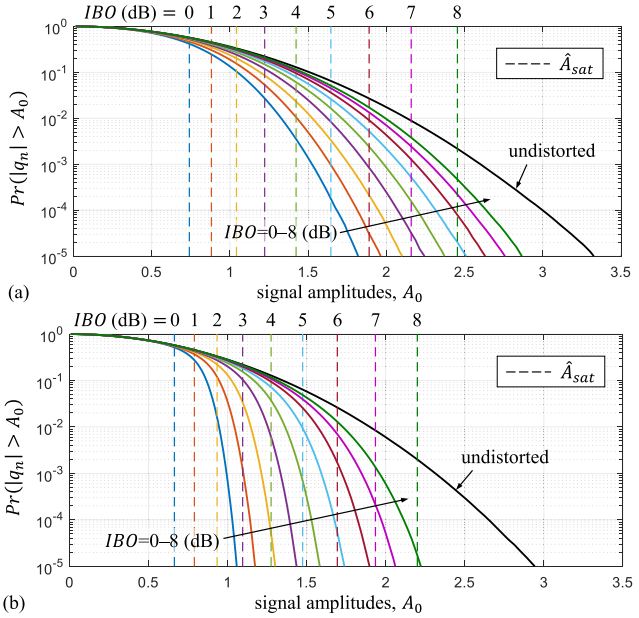

FIGURE 4. CCDF of $|q_n|$ for estimating $\mathcal{L}_D^{ISR}$ over AWGN channel with (a) $E_b/N_0 = 0$ dB (b)$E_b/N_0 = 20$ dB.

By matching the criterion $\mathcal{L}_D^{ISR} \leq 25\%$, the smallest IBO is 2 dB according to the $\mathcal{L}_D^{ISR}$ values marked with red color in Table 2. However, the analysis in [33] indicates that both the signal noise and iteration limit will degrade the performance of SC, making the maximum value of $\mathcal{L}_D^{ISR}$ smaller than 25%, i.e., $\mathcal{K}_T^{ISR}$. Therefore, effective SC may occur when the IBO is not lower than 3 dB. (Refer to the $\mathcal{L}_D^{ISR}$ values marked with blue color in Table 2.)

TABLE 2. Time-Domain Lost-Knowledge Ratio (%) Versus IBO and Normalized SNR

IBO [dB]	E_b/N_0 [dB]					undistorted
	0	5	10	15	20	
0	43.1105	47.6518	50.9835	52.2034	52.5642	52.7401
1	31.5195	33.8598	36.1367	37.2726	37.6483	37.8244
2	20.8746	21.1574	21.8982	22.4990	22.7477	22.8544
3	12.2264	11.2761	10.8340	10.7607	10.7704	10.7842
4	6.1393	4.9494	4.1839	3.8467	3.7300	3.6785
5	2.5423	1.7208	1.2183	0.9935	0.9112	0.8734
6	0.8287	0.4532	0.2620	0.1863	0.1609	0.1480
7	0.1987	0.0849	0.0394	0.0255	0.0208	0.0188
8	0.0326	0.0104	0.0041	0.0023	0.0020	0.0018

The simulations are based on CBW1 parameterization in 802.11ah standard ($N = 32$, $N_d = 24$, $N_p = 2$, and $N_n = 6$).

D. COMPLEXITY ANALYSIS

Based on the elaboration of frequency-domain and time-domain prior knowledge, we summarize the whole process of the proposed ISR in Fig. 5. The computational complexity of the proposed schemes, ISR-I and ISR-II, are expressed in the big-O notation which is related to the number of subcarriers of OFDM symbols [39]. From Algorithm 1, the ISR scheme in each iteration is subject to complexity $\mathcal{O}\left(2N \log_2 N\right)$ to

Input: $\boldsymbol{q}$, IBO, δ

$\hat{A}_{sat} = q_{RMS} \cdot 10^{IBO/20}$ (12)

$[\mathcal{J}_D^{ISR}]_{(j,j)} = \begin{cases} 1, & q_n < \hat{A}_{sat} \\ 0, & q_n \geq \hat{A}_{sat} \end{cases}, 0 \leq j, n \leq N-1$ (13)

$\boldsymbol{K}_D^{ISR} = \boldsymbol{\mathcal{J}}_D^{ISR}\boldsymbol{q}$ (14)

$\widehat{\boldsymbol{q}}^{(i=0)} = \boldsymbol{q}$ // Initial guess

while $NMSE(\widehat{\boldsymbol{q}}^{(i)}) < \delta$ **do**

  // Applying frequency-domain prior knowledge

  if ISR-I is used **then**

    $\widehat{\boldsymbol{q}}^{(i+1)} = \mathcal{F}_N^H\left[\left(\boldsymbol{I} - \boldsymbol{\mathcal{J}}_T^{ISR}\right)\widehat{\boldsymbol{Q}}^{(i)} + \boldsymbol{K}_T^{ISR}\right]$ (11a)

  end if

  if ISR-II is used **then**

    $\widehat{\boldsymbol{q}}^{(i+1)} = \mathcal{F}_N^H\left[\left(\boldsymbol{I} - \boldsymbol{\mathcal{J}}_T^{ISR}\right)\boldsymbol{Q}_{HD}^{(i)} + \boldsymbol{K}_T^{ISR}\right]$ (11b)

  end if

  // Applying time-domain prior knowledge

  $\widehat{\boldsymbol{q}}^{(i+1)} = \left(\boldsymbol{I} - \boldsymbol{\mathcal{J}}_D^{ISR}\right)\widehat{\boldsymbol{q}}^{(i+1)} + \boldsymbol{K}_D^{ISR}$

end while

Output: $\widehat{\boldsymbol{q}}^{(i)}$

FIGURE 5. Algorithm of iterative subcarrier regularization.

perform the FFT/IFFT pair and $\mathcal{O}(2N)$ to update the prior knowledge in both domains. As ISR-II in (11b) needs to perform hard decision for N_d data subcarriers to obtain $\boldsymbol{Q}_{\boldsymbol{HD}}^{(i)}$ with extra complexity $\mathrm{O}(N_d M)$, the computational complexity with i_t iterations for ISR-I and ISR-II can be summarized as $\mathcal{O}\left(2N\left(\log_2 N + 1\right) i_t\right)$ and $\mathcal{O}\left(2N\left(\log_2 N + 1\right) i_t + N_d \mathcal{M} i_t\right)$, respectively. Note that the value of N_d refers to the parameterization of 802.11ah protocol.

Consequently, the resulting complexity shows that the additional complexity of the receiver for AP with ISR only comes from the reuse of functions of FFT and hard decision and is mainly dominated by the number of iterations. The proposed scheme can be seamlessly incorporated into 802.11ah chips as longer processing time is tolerant in IoT networking.

E. PERFORMANCE EVALUATION

The evaluation of ISR restoration performance with 802.11ah CBW1 parameterization is presented as follows. As ISR is an iterative nonlinear process whose two random variables, converged iteration times (denoted as i_c) and converged NMSE between restored and original signal (denoted as $NMSE_{i_c} = \left\|\boldsymbol{x} - \hat{\boldsymbol{v}}^{(i_c)}\right\|_2^2 / \|\boldsymbol{x}\|_2^2$), are hard to be analytically featured, we empirically evaluate their performance in terms of two-dimensional joint probability density function (PDF), denoted as $f_{i_c, NMSE_{i_c}}(a, b)$, versus different IBO values. Here, the converge threshold δ is set to 10^{-6} and 5×10^5 random OFDM symbols are tested.

Fig. 6 shows the PDF of $f_{i_c, NMSE_{i_c}}(a, b)$ in $IBO = 1-5$ dB for ISR-I and ISR-II schemes with different initial guesses (zeros/received samples). Clearly, the largest variances of i_c and $NMSE_{i_c}$ appear at $IBO = 2$ dB for all the considered schemes because the corresponding ratio of time-domain knowledge ($\mathcal{K}_T^{ISR}$) is near to $\mathcal{L}_D^{ISR}$ (see Table 2). In the view of convergence, it can be found that setting initial guesses as received samples is faster than setting as zeros (50–200 iterations reduce to 50–100 iterations). The ISR-II scheme is faster than ISR-I (50–100 iterations reduce to 1–10 iterations) because of the aid of hard decisions for $1 - \mathcal{K}_T^{ISR} = 75\%$ subcarriers that transfer QAM data. The presence of AWGN nearly does not influence the convergence of ISR-II scheme. For the convergent NMSE, the lowest NMSE of $IBO = 1$ dB is worse than that of $IBO = 2-5$ dB since the former does not satisfy the criterion $\mathcal{L}_D^{ISR} \leq \mathcal{K}_T^{ISR}$ [33]. Therefore, the distributions of converged NMSE between $IBO = 2-5$ dB are almost identical because the presence of the noise is the only factor to control the performance of converged NMSE when $\mathcal{L}_D^{ISR} \leq \mathcal{K}_T^{ISR}$ (i.e., all time-domain lost-knowledge ratios are smaller than 25% for $IBO = 2-5$ dB as presented in Table 2). Based on these findings, the simulations in the subsequent section will be only discussed in the case of $IBO > 2$ dB.

IV. SIMULATION RESULTS AND DISCUSSION

A Monte Carlo simulation is conducted to verify the proposed SC scheme regarding a number of performance metrics, including power spectral density (PSD), BER, total degradation (TD) and convergence. Based on these results, an estimation on the PA efficiency improvement is provided. The same 802.11ah-CBW1 parametrization used in Section III-E is adopted in the simulation, i.e., $N = 32$ subcarriers including 2 pilot subcarriers, 6 null subcarriers, and 24 data subcarriers (using 16-QAM constellation).

A. POWER SPECTRAL DENSITY

The nonlinearity of transmit PA may cause out-of-band noise and increase the adjacent channel leakage power. Thus, the spectral mask will be crucial to determine the PA efficiency. Fig. 7 depicts the spectral mask and the PSD under different IBO values, where the unit "dBr" therein denotes dB value relative to the maximum spectral density of the signal. It can be found that the lowest IBO, which does not exceed the spectral mask, is 3 dB. This IBO value is exactly equal to the estimated recovery boundary of ISR which is also shown in Section III-C, and it implies that the minimum IBO of the transmit PA that achieves maximum power saving is 3 dB under 802.11ah CBW1 system parameters.

B. BIT ERROR RATE

Although 802.11ah uses binary convolutional code or low-density parity-check code to enhance the BER, the uncoded BER performance is provided in this study to observe the pure contributions of considered schemes. The simulation is over a Rayleigh fading channel with $L = P = N/4$ resolvable paths [5]. Fig. 8 shows that the proposed SC schemes can effectively reduce the BER and ISR-II constantly outperforms ISR-I by taking $IBO = 3$ dB. Although ISR takes more iterations to converge in the NMSE performance (Section III-E), Fig. 8 shows that ISR-II can achieve considerable BER improvement with the aid of constellation tolerance by taking only two iterations. Like most of the other

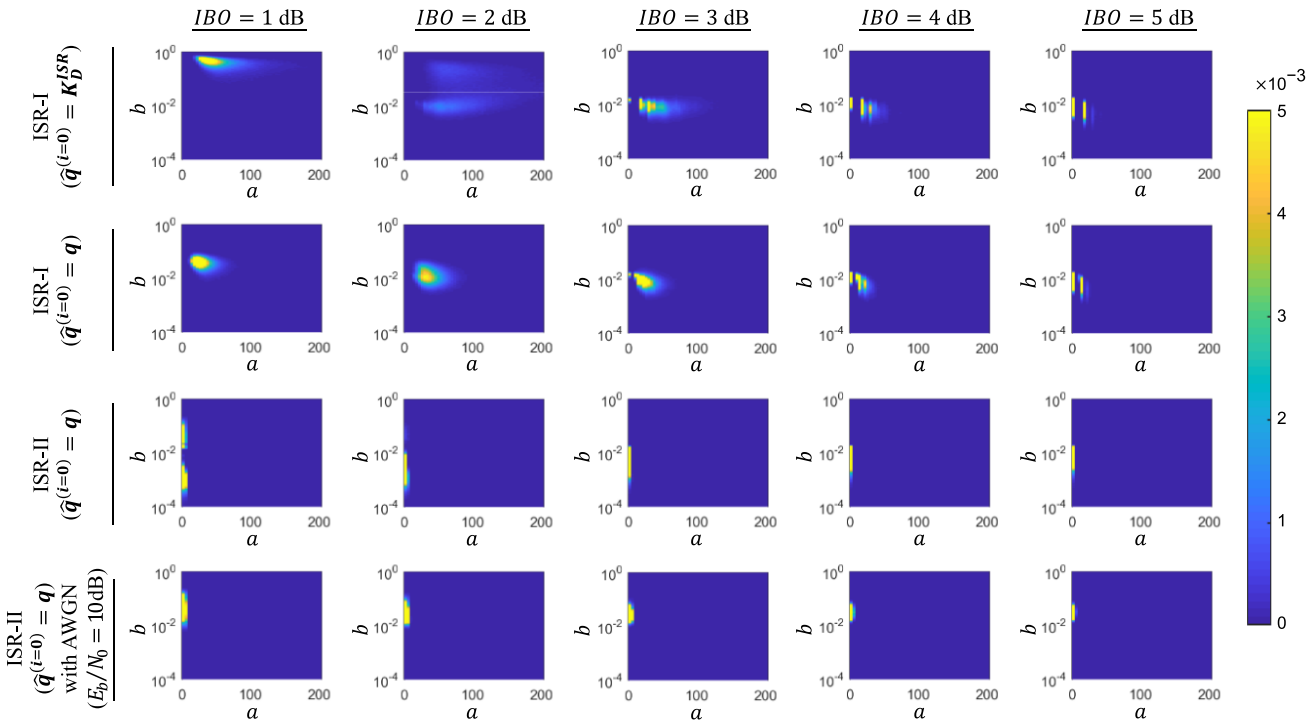

FIGURE 6. Joint PDF of convergent number of iteration and its NMSE ($f_{i_C,NMSE_{i_C}}(a,b)$) in $IBO = 1-5$ dB for ISR-I and ISR-II schemes with different initial guesses.

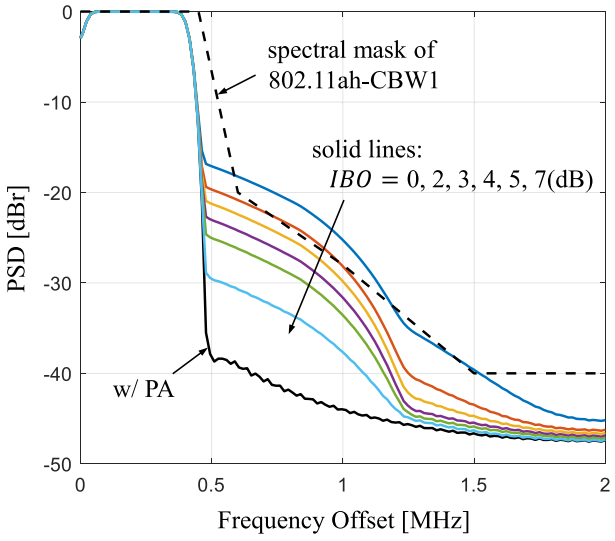

FIGURE 7. Comparison of PSD with different IBOs.

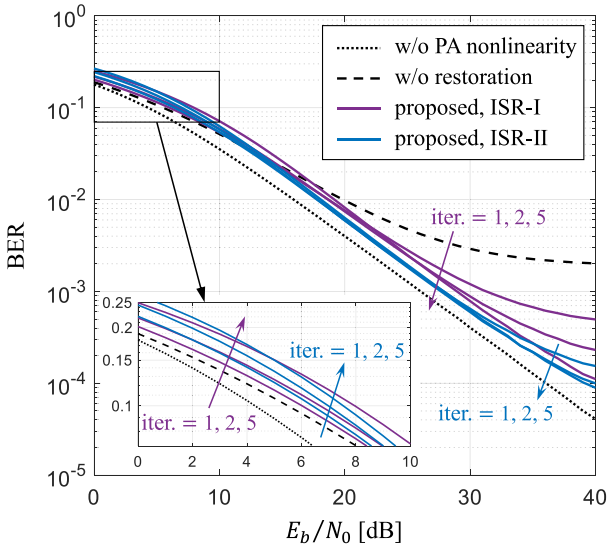

FIGURE 8. BER comparison of the proposed ISR with $IBO = 3$dB and 16-QAM over Rayleigh fading channel.

SC schemes, the proposed ISR has to work under relatively high SNR ($E_b/N_0 \geq 15$ dB) and otherwise may lead to even worse BER performance when more iterations are launched due to the imperfection of time-domain prior knowledge. This impact follows the PSD results shown in the last two rows of subfigures in Fig. 6. The presence of noise would increase the NMSE of converged symbol data and further degrade the BER performance. ISR-II suffers from such performance impairment as it is more sensitive to any error decision. Therefore, it is an effective strategy for the transmitter to determine whether ISR is activated for achieving high PA-efficiency according to the received CSI.

Fig. 9 and 10 show the comparison results between the proposed ISR-II and two types of signal models for ICNC: ICNC with or without CF before PA nonlinearity at transmitters. Considering the clipping level $A_{clip} = A_{sat}$ for ICNC with $IBO = 3$ dB, Fig. 9 shows that ISR-II is subject to

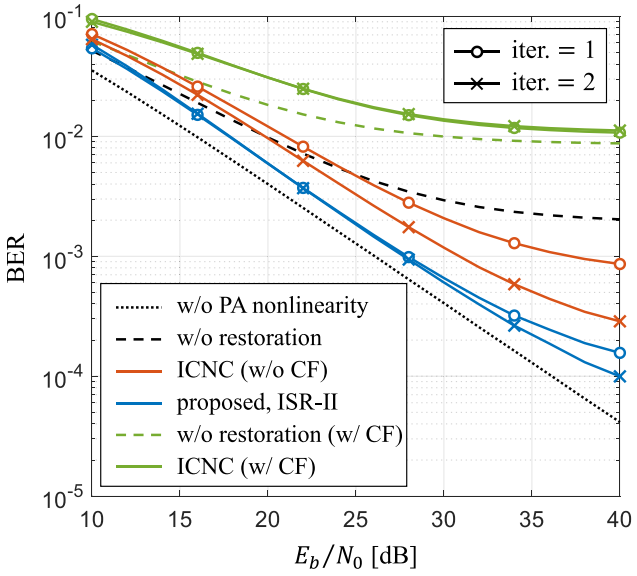

FIGURE 9. BER comparison of ISR and ICNC with *IBO* = 3dB and 16-QAM over Rayleigh fading channel.

only 2-dB SNR lower than the ideal case (i.e., without PA nonlinearity), and such performance is achieved with only one iteration at BER = 10^{-3}. This is compared with the case of ICNC without CF that is subject to 11-dB lower SNR. Note that the proposed ISR-II utilizes "soft clipping (PA nonlinearity)" instead of "hard clipping" at the transmitters, such that the estimation of clipping noise in ICNC would be no longer accurate and thus degrades the performance. Consequently, ICNC with CF is also examined. It shows that with more iterations does not improve the BER because truncating 3 dB of transmitted signals and passing through the PA nonlinearity severely deteriorate the orthogonality of subcarriers. Fig. 10 demonstrates that with *IBO* = 4 dB,

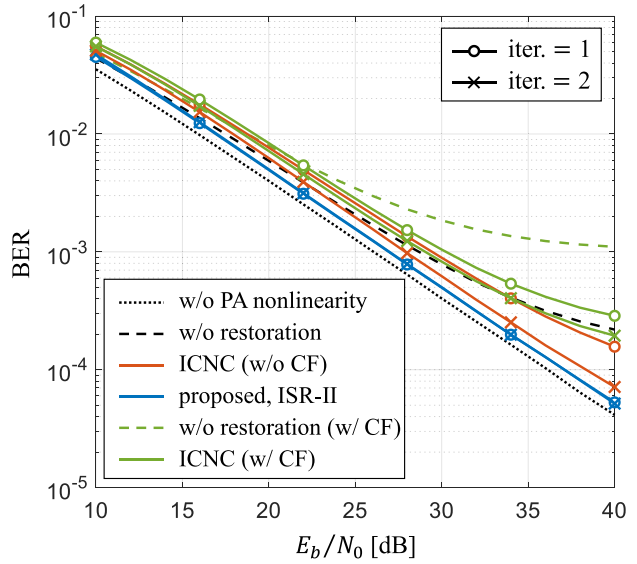

FIGURE 10. BER comparison of ISR and ICNC with *IBO* = 4dB and 16-QAM over Rayleigh fading channel.

the ICNC with CF can compensate the signals successfully while it still performs worse than that case without CF. The performance of ISR-II continues to outperform ICNC under all the considered IBO values and numbers of iterations. Note that with IBO over 4 dB, ISR-II of two iterations yields very limited BER improvement against that by taking one according to Fig. 10; and thus the best strategy in this case is to take one iteration to achieve the best cost-performance value.

C. TOTAL DEGRADATION

Let the degradation of power efficiency due to the nonlinear effect be denoted as *TD* (in dB), which quantifies the difference between the maximum power of PA and the input power of a linear amplifier required to assure a predefined BER)) [40]. TD is expressed as follows:

$$TD\,[dB] = IBO + \left(\frac{E_b}{N_0}\right)_{nonlin.} - \left(\frac{E_b}{N_0}\right)_{lin.}, \qquad (15)$$

where $(E_b/N_0)_{lin.}$ and $(E_b/N_0)_{nonlin.}$ denote as the required SNRs in linear PA and nonlinear PA, respectively. Fig. 11 presents the TD performance corresponding to the same study cases of Figs. 9 and 10, with a BER target of 10^{-3}, which is sufficient to enable forward error correction (FEC) in the linear channel with AWGN. It is seen that the smallest TD (at about 4–5 dB) appears at $IBO = 3 - 4$ dB. This outcome advocates the analysis result of BER performance, showing that the proposed ISR schemes yield the best performance at $IBO = 3 - 4$ dB.

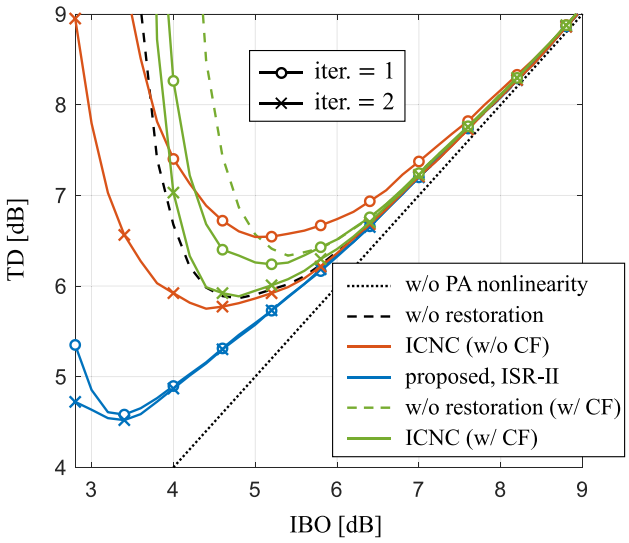

FIGURE 11. TD comparison of ISR and ICNC for 16-QAM with target BER = 10^{-3} over Rayleigh fading channel.

D. POWER SAVING EVALUATION

The IBO employed at the 802.11ah PA is usually 8–12dB when being considered for the micro-/pico-cell usage, leading to low PA efficiency [41]. To evaluate the power saving, we consider a linear PA (e.g., Class A and Class B) where

linear amplification can be achieved up to the saturation point. We define the actual PA efficiency $\eta = \eta_{max}/PAPR$ [42] for power saving measure, where η_{max} is the maximum PA efficiency. The value of PAPR is linearly scaled with IBO as the probability of saturated samples is directionally related to on recovery ability of SC-based schemes. Accordingly, the improvement ratio of PA efficiency can be expressed as

$$\Delta\eta = 10\log_{10}\left(\frac{\eta_2}{\eta_1}\right) = 10\log_{10}\left(\frac{IBO_1}{IBO_2}\right), \quad (16a)$$

or

$$\Delta\eta = [IBO_1]_{dB} - [IBO_2]_{dB}\,, \quad (16b)$$

where η_1 and η_2 is the PA efficiency for IBO_1 and IBO_2 ($IBO_1 > IBO_2$), respectively. All the simulation results of PSD, BER, and TD indicate that the IBO can be reduced from 8–12 dB to 3–4 dB by applying the proposed scheme (ISR-II) with a fair SNR ($E_b/N_0 \geq 10$ dB). From (16b), we conclude that our schemes improve the PA efficiency in the range of 4–9 dB; i.e., $\Delta\eta = [8, 12] - [3, 4] = [4, 9]$ dB. Such improvement significantly mitigates the PA power consumption and thus is expected to solidly extend the battery lifespan of 802.11ah IoT-CDs.

E. CONVERGENCE

Follow the system parameters used in Fig. 9, Fig. 12 shows the numerical results of convergence performance in terms of the number of iterations versus BER. For a fair channel ($E_b/N_0 = 15$ dB), the proposed ISR-I and ISR-II achieve a minimal BER at $i = 1$ but converge to a higher BER when i increases owing to the impact of distorted time-domain prior knowledge. Notwithstanding, both BERs still outperform ICNC at $i = 1$.

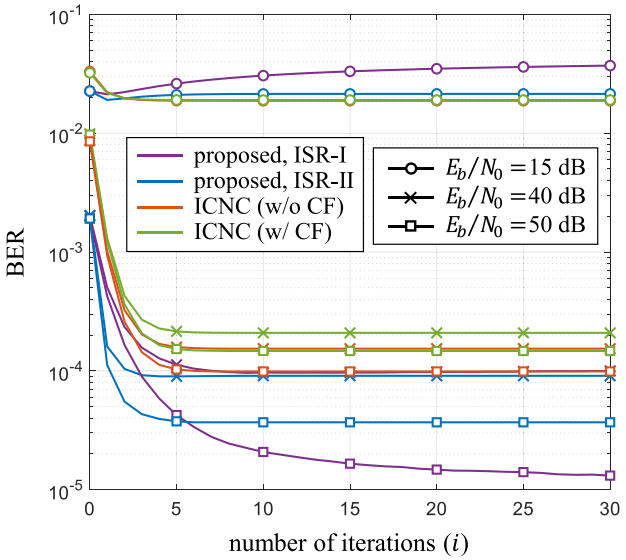

FIGURE 12. Convergence comparison of ISR and ICNC with *IBO* = 3dB and 16-QAM over Rayleigh fading channel.

For a good channel ($E_b/N_0 = 40$ dB), the ISR-II and ICNC converge at $i = 3$ and $i = 5$, respectively, whilst ISR-I at $i = 10$ due to the fact that ISR-I updates only $\mathcal{K}_T^{ISR} = 25\%$ subcarrier data in each iteration. In the viewpoint of BER, the performance of ISR-II keeps superior to the others at any number of iteration. It is interesting to find that with a higher channel quality (e.g., $E_b/N_0 = 50$ dB shown in Fig. 12), the converged BER of ISR-I can be further reduced by consuming more iterations. This finding highlights the ISR-I on its potential for robust reconstruction when the conditions of time resource and channel quality are satisfied.

V. CONCLUDING REMARKS

For an IoT-CD, the power consumption by uplink transmissions highly depends on the output power of the transmitter, which is in turn determined by the PA's IBO. This article introduces an SC scheme, namely ISR, aiming to solidly reduce the required IBO of the uplink transmission for IoT CDs under the 802.11ah specification. To enable effective signal reconstruction, the ISR is based on GPGA that can handle any signal. We claim that the proposed ISR scheme can completely incorporate with the current industrial specification and 802.11ah CDs since all the required prior information and processing, including iterative FFT and hard decision operations, are inherently available in the CDs via system-built-in functions in the RF module. Note that although this study positioned ISR in the scenario of 802.11ah, it can be generalized to any OFDM system with some subcarriers carrying the prior channel knowledge. Simulation results demonstrate that the proposed scheme can significantly reduce the required IBO up to 3–4 dB with 4–5 dB TD (target uncoded BER is $\mathbf{10^{-3}}$), leading to 4–9 dB improvement of PA efficiency for uplink signaling.

The adaptivity of ISR superiors to ICNC-based schemes because ISR can work in any PA type that poses high nonlinearity at large amplitudes and low nonlinearity at small ones. However, the strategy of disabling or applying ISR-I or ISR-II according to the available time resource of AP and channel quality is still to be further investigated for performance optimization. This should be considered with the modulation coding scheme described in 802.11ah. Given that most SC schemes in recent years had been proposed for improving the coding technique of IEC [30], there is a great potential for ISR to combine those schemes against imperfect CSI such as estimation errors and propagation delays. On the other hand, we notice that ISR may be also applied to counteract impulsive noise mitigation (e.g., [43]–[45]), which is another important issue for OFDM nonlinearity. Both issues will be considered as our future works.

REFERENCES

[1] A. Ikpehai, B. Adebisi, K. M. Rabie, K. Anoh, R. E. Ande, M. Hammoudeh, H. Gacanin, and U. M. Mbanaso, "Low-power wide area network technologies for Internet-of-Things: A comparative review," *IEEE Internet Things J.*, vol. 6, no. 2, pp. 2225–2240, Apr. 2019, doi: 10.1109/JIOT.2018.2883728.

[2] H. Wang and A. O. Fapojuwo, "A survey of enabling technologies of low power and long range machine-to-machine communications," *IEEE Commun. Surveys Tuts.*, vol. 19, no. 4, pp. 2621–2639, 4th Quart., 2017, doi: 10.1109/COMST.2017.2721379.

[3] L. Chettri and R. Bera, "A comprehensive survey on Internet of Things (IoT) toward 5G wireless systems," *IEEE Internet Things J.*, vol. 7, no. 1, pp. 16–32, Jan. 2020, doi: 10.1109/JIOT.2019.2948888.

[4] *Standardization of NB-IOT Completed*. Accessed: Jun. 18, 2019. [Online]. Available: https://www.3gpp.org/news-events/3gpp-news/1785-nb_iot

[5] *Standard for Information Technology–Telecommunications and Information Exchange Between Systems-Local and Metropolitan Area Networks–Specific Require. S.l.*, IEEE Stabdard 802.11ah-2016 (Amendment to IEEE Std 802.11-2016, as amended by IEEE Std 802.11ai-2016), 2017.

[6] A. Rico-Alvarino, M. Vajapeyam, H. Xu, X. Wang, Y. Blankenship, J. Bergman, T. Tirronen, and E. Yavuz, "An overview of 3GPP enhancements on machine to machine communications," *IEEE Commun. Mag.*, vol. 54, no. 6, pp. 14–21, Jun. 2016, doi: 10.1109/MCOM.2016.7497761.

[7] Y. Rahmatallah and S. Mohan, "Peak-to-average power ratio reduction in OFDM systems: A survey and taxonomy," *IEEE Commun. Surveys Tuts.*, vol. 15, no. 4, pp. 1567–1592, 4th Quart., 2013, doi: 10.1109/SURV.2013.021313.00164.

[8] *Technical Specification Group Radio Access Network; Evolved Universal Terrestrial Radio Access (E-UTRA); Physical Channels and Modulation (Release 15)*, document TS 36.211 V15.4.0, 3GPP, 2018.

[9] X. Yu, M. Wei, Y. Yin, Y. Song, Z. Wang, Y. Sun, and B. Chi, "A sub-GHz low-power transceiver with PAPR-tolerant power amplifier for 802.11ah applications," in *Proc. IEEE Radio Freq. Integr. Circuits Symp. (RFIC)*, Phoenix, AZ, USA, May 2015, pp. 231–234, doi: 10.1109/RFIC.2015.7337747.

[10] N. Andrade, P. Toledo, G. Guimaraes, H. Klimach, H. Dornelas, and S. Bampi, "Low power IEEE 802.11ah receiver system-level design aiming for IoT applications," in *Proc. Symp. Integr. Circuits Syst. Design (SBCCI)*, Fortaleza, Brazil, 2017, pp. 11–16, doi: 10.1145/3109984.3110013.

[11] M. Wei, Z. Song, P. Li, J. Lin, J. Zhang, J. Hao, and B. Chi, "A fully integrated reconfigurable low-power sub-GHz transceiver for 802.11ah in 65nm CMOS," in *Proc. IEEE Radio Freq. Integr. Circuits Symp. (RFIC)*, Honolulu, HI, USA, Jun. 2017, pp. 240–243, doi: 10.1109/RFIC.2017.7969062.

[12] Y. Zhao, O. N. C. Yilmaz, and A. Larmo, "Optimizing M2M energy efficiency in IEEE 802.11ah," in *Proc. IEEE Globecom Workshops (GC Wkshps)*, San Diego, CA, USA Dec. 2015, pp. 1–6, doi: 10.1109/GLOCOMW.2015.7414004.

[13] L. Beltramelli, P. Österberg, U. Jennehag, and M. Gidlund, "Hybrid MAC mechanism for energy efficient communication in IEEE 802.11ah," in *Proc. IEEE Int. Conf. Ind. Technol. (ICIT)*, Toronto, ON, Canada, Mar. 2017, pp. 1295–1300, doi: 10.1109/ICIT.2017.7915550.

[14] T. Kim and J. Morris Chang, "Enhanced power saving mechanism for large-scale 802.11ah wireless sensor networks," *IEEE Trans. Green Commun. Netw.*, vol. 1, no. 4, pp. 516–527, Dec. 2017, doi: 10.1109/TGCN.2017.2727056.

[15] E. Khorov, A. Krotov, A. Lyakhov, R. Yusupov, M. Condoluci, M. Dohler, and I. Akyildiz, "Enabling the Internet of Things with Wi-Fi Halow—Performance evaluation of the restricted access window," *IEEE Access*, vol. 7, pp. 127402–127415, 2019, doi: 10.1109/ACCESS.2019.2939760.

[16] E. Olfat and M. Bengtsson, "Joint channel and clipping level estimation for OFDM in IoT-based networks," *IEEE Trans. Signal Process.*, vol. 65, no. 18, pp. 4902–4911, Sep. 2017, doi: 10.1109/TSP.2017.2713765.

[17] L. Cho, X.-H. Yu, C.-Y. Chen, and C.-Y. Hsu, "Green OFDM for IoT: Minimizing IBO subject to a spectral mask," in *Proc. IEEE Int. Conf. Appl. Syst. Invention (ICASI)*, Chiba, Japan, Apr. 2018, pp. 5–8, doi: 10.1109/ICASI.2018.8394252.

[18] T.-C. Chang, C.-H. Lin, K. Ching-Ju Lin, and W.-T. Chen, "Traffic-aware sensor grouping for IEEE 802.11ah networks: Regression based analysis and design," *IEEE Trans. Mobile Comput.*, vol. 18, no. 3, pp. 674–687, Mar. 2019, doi: 10.1109/TMC.2018.2840692.

[19] E. Al-Dalakta, A. Al-Dweik, A. Hazmi, C. Tsimenidis, and B. Sharif, "PAPR reduction scheme using maximum cross correlation," *IEEE Commun. Lett.*, vol. 16, no. 12, pp. 2032–2035, Dec. 2012, doi: 10.1109/LCOMM.2012.101712.122151.

[20] E. Al-Dalakta, A. Al-Dweik, A. Hazmi, C. Tsimenidis, and B. Sharif, "Efficient BER reduction technique for nonlinear OFDM transmission using distortion prediction," *IEEE Trans. Veh. Technol.*, vol. 61, no. 5, pp. 2330–2336, Jun. 2012, doi: 10.1109/TVT.2012.2190950.

[21] J. Armstrong, "Peak-to-average power reduction for OFDM by repeated clipping and frequency domain filtering," *Electron. Lett.*, vol. 38, no. 5, p. 246, 2002, doi: 10.1049/el:20020175.

[22] Y. Sui, Y. He, T. Cheng, Y. Huang, Y. Wu, L. Shi, and A. Farhan, "Adaptive elastic echo state network for channel prediction in IEEE802.11ah standard-based OFDM system," *IEEE Access*, vol. 8, pp. 10169–10185, 2020, doi: 10.1109/ACCESS.2020.2964810.

[23] *Technical Specification Group Radio Access Network; Study on Provision of Low-Cost Machine-Type Communications (MTC) User Equipments (UEs) Based on LTE (Release 12)*, document TR 36.888 V12.0.0, 3GPP, Jun. 2013.

[24] J. Tellado, L. M. C. Hoo, and J. M. Cioffi, "Maximum-likelihood detection of nonlinearly distorted multicarrier symbols by iterative decoding," *IEEE Trans. Commun.*, vol. 51, no. 2, pp. 218–228, Feb. 2003, doi: 10.1109/TCOMM.2003.809289.

[25] J. Guerreiro, R. Dinis, and P. Montezuma, "Optimum and sub-optimum receivers for OFDM signals with strong nonlinear distortion effects," *IEEE Trans. Commun.*, vol. 61, no. 9, pp. 3830–3840, Sep. 2013, doi: 10.1109/TCOMM.2013.072913.120344.

[26] N. Regev, I. Iofedov, and D. Wulich, "Maximum likelihood detection of nonlinearly distorted OFDM signal," in *Proc. IEEE Global Commun. Conf. (GLOBECOM)*, San Diego, CA, USA, Dec. 2015, pp. 1–6, doi: 10.1109/GLOCOM.2015.7417009.

[27] H. Chen and A. M. Haimovich, "Iterative estimation and cancellation of clipping noise for OFDM signals," *IEEE Commun. Lett.*, vol. 7, no. 7, pp. 305–307, Jul. 2003, doi: 10.1109/LCOMM.2003.814720.

[28] I. Gutman, I. Iofedov, and D. Wulich, "Iterative decoding of iterative clipped and filtered OFDM signal," *IEEE Trans. Commun.*, vol. 61, no. 10, pp. 4284–4293, Oct. 2013, doi: 10.1109/TCOMM.2013.090513.120983.

[29] L. Yang, K. Song, and Y. M. Siu, "Iterative clipping noise recovery of OFDM signals based on compressed sensing," *IEEE Trans. Broadcast.*, vol. 63, no. 4, pp. 706–713, Dec. 2017, doi: 10.1109/TBC.2017.2669641.

[30] S. Liang, J. Tong, and L. Ping, "On iterative compensation of clipping distortion in OFDM systems," *IEEE Wireless Commun. Lett.*, vol. 8, no. 2, pp. 436–439, Apr. 2019, doi: 10.1109/LWC.2018.2874935.

[31] R. W. Gerchberg, "Super-resolution through error energy reduction," *Optica Acta, Int. J. Opt.*, vol. 21, no. 9, pp. 709–720, Sep. 1974, doi: 10.1080/713818946.

[32] A. Papoulis, "A new algorithm in spectral analysis and band-limited extrapolation," *IEEE Trans. Circuits Syst.*, vol. 22, no. 9, pp. 735–742, Sep. 1975, doi: 10.1109/TCS.1975.1084118.

[33] L. Cho, C.-Y. Chen, C.-K. Lin, and C.-Y. Hsu, "The convergence analysis of extended Papoulis-Gerchberg algorithm on AWGN-smeared signals," in *Proc. IEEE Int. Conf. Appl. Syst. Invention (ICASI)*, Chiba, Japan, Apr. 2018, pp. 730–733, doi: 10.1109/ICASI.2018.8394363.

[34] E. Brugnoli, E. Toscano, and C. Vetro, "Iterative reconstruction of signals on graph," *IEEE Signal Process. Lett.*, vol. 27, pp. 76–80, 2020, doi: 10.1109/LSP.2019.2956670.

[35] D. Kim and G. L. Stuber, "Clipping noise mitigation for OFDM by decision-aided reconstruction," *IEEE Commun. Lett.*, vol. 3, no. 1, pp. 4–6, Jan. 1999, doi: 10.1109/4234.740112.

[36] C. Rapp, "Effect of HPA-nonlinearity on 4-DPSK/OFDM-signal for a digital sound broadcasting system," in *Proc. Eur. Conf. Satell. Commun.*, Liege, Belgium, vol. 2, Oct. 1991, pp. 179–184.

[37] R. Marks, "Restoring lost samples from an oversampled band-limited signal," *IEEE Trans. Acoust., Speech, Signal Process.*, vol. 31, no. 3, pp. 752–755, Jun. 1983, doi: 10.1109/TASSP.1983.1164101.

[38] H. Woo Kang, Y. Soo Cho, and D. Hee Youn, "On compensating nonlinear distortions of an OFDM system using an efficient adaptive predistorter," *IEEE Trans. Commun.*, vol. 47, no. 4, pp. 522–526, Apr. 1999, doi: 10.1109/26.764925.

[39] Y.-C. Wang and Z.-Q. Luo, "Optimized iterative clipping and filtering for PAPR reduction of OFDM signals," *IEEE Trans. Commun.*, vol. 59, no. 1, pp. 33–37, Jan. 2011, doi: 10.1109/TCOMM.2010.102910.090040.

[40] S. C. Thompson, J. G. Proakis, and J. R. Zeidler, "The effectiveness of signal clipping for PAPR and total degradation reduction in OFDM systems," in *Proc. IEEE Global Telecommun. Conf. (GLOBECOM)*, St. Louis, MO, USA, 2005, pp. 2807–2811, doi: 10.1109/GLOCOM.2005.1578271.

[41] A. Gunther *et al.*, "EARTH deliverable D2.3—Energy efficiency analysis of the reference systems, areas of improvements and target breakdown," Brussels, Belgium, Tech. Rep. INFSO-ICT-247733, Jan. 2012. Accessed: Jan. 15, 2021. [Online]. Available: https://cordis.europa.eu/docs/projects/cnect/3/247733/080/deliverables/001-EARTHWP2D23v2.pdf

[42] R. J. Baxley and G. T. Zhou, "Power savings analysis of peak-to-average power ratio reduction in OFDM," *IEEE Trans. Consum. Electron.*, vol. 50, no. 3, pp. 792–798, Aug. 2004, doi: 10.1109/TCE.2004.1341681.
[43] S. V. Zhidkov, "Performance analysis and optimization of OFDM receiver with blanking nonlinearity in impulsive noise environment," *IEEE Trans. Veh. Technol.*, vol. 55, no. 1, pp. 234–242, Jan. 2006, doi: 10.1109/TVT.2005.858191.
[44] S. V. Zhidkov, "Analysis and comparison of several simple impulsive noise mitigation schemes for OFDM receivers," *IEEE Trans. Commun.*, vol. 56, no. 1, pp. 5–9, Jan. 2008, doi: 10.1109/TCOMM.2008.050391.
[45] D. Darsena, G. Gelli, F. Melito, and F. Verde, "ICI-free equalization in OFDM systems with blanking preprocessing at the receiver for impulsive noise mitigation," *IEEE Signal Process. Lett.*, vol. 22, no. 9, pp. 1321–1325, Sep. 2015, doi: 10.1109/LSP.2015.2398366.

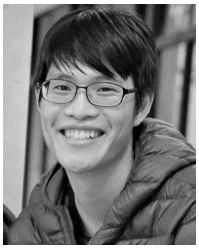

LI CHO (Member, IEEE) received the B.S. degree in electrical engineering and the M.S. and Ph.D. degrees in communication engineering from Tatung University, Taipei, Taiwan, in 2009, 2010, and 2020, respectively. From 2019 to 2020, he was an Adjunct Instructor with the Department of Electrical Engineering. Since 2016, he has been the Center of Wireless Broadband Technology, Tatung University. Since August 2020, he has also been with Chunghwa Telecom Company. His research interests include multicarrier communications, index modulation, signal restoration algorithms, and machine learning.

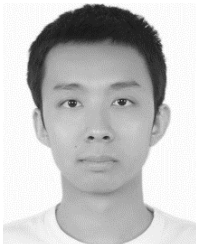

XIANHUA YU (Student Member, IEEE) received the B.S. and M.S. degrees in electrical engineering from Tatung University, Taipei, Taiwan, in 2017 and 2020, respectively. Since 2016, he joined the Center of Wireless Broadband Technology, Tatung University. His research interests include signal restoration algorithms, multicarrier communications, and machine learning.

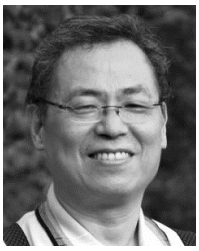

CHAU-YUN HSU (Member, IEEE) received the B.S., M.S., and Ph.D. degrees in electrical engineering from the Tatung Institute of Technology, Taipei, Taiwan, in 1981, 1983, and 1988, respectively. From 1983 to 1985, he was a Lecturer of the faculties of the Department of Electrical Engineering, Tatung University. From 1988 to 1998, he served as the Associate Professor. From 2002 to 2008, he also served as the Chair for the Department of Electrical Engineering. From 2009 to 2012, he also served as the Dean for research and development of Tatung University. He is currently the Professor of the Graduate Institute of Communication Engineering and also the Dean of College of Electrical Engineering and Computer Science, Tatung University. His current interests include wireless channel model, machine learning, digital signal processing, and image processing.

PIN-HAN HO (Fellow, IEEE) received the Ph.D. degree from Queen's University, Kingston, ON, Canada, in 2002. He is currently a Full Professor with the Department of Electrical and Computer Engineering, University of Waterloo, ON, Canada. He has authored and coauthored more than 350 refereed technical articles, several book chapters, and two books on optical networking and survivability. His current research interests include a wide range of topics in broadband wired and wireless communication technologies.

Dr. Ho was a recipient of the Distinguished Research Excellence Award in the ECE Department of University of Waterloo, Early Award (Premier Research Excellence Award), in 2005, the Best Paper Award in SPECTS'02, ICC'05 Optical Networking Symposium, the ICC'07 Security and Wireless Communications Symposium, and the Outstanding Paper Award in HPSR02.